CHAPTER III
RESULTS AND DISCUSSION

3.1 Rheological Characterizations

3.1.1 Molecular Weight Characterization

Table 3.1 shows the molecular weights of PP, HDPE(1), HDPE (2), PS, and PMMA characterized by the cone and plate rheometer using the Orchestrator program. The weight average molecular weight data of the homopoymers are close to the values quoted from company (Table 2.1). The weight average molecular weight values of PP, PS, and HDPE(1) are close to each other. HDPE(2) has the lowest molecular weights (M_w, M_n, and M_z).

Table 3.1 The molecular weights of the five polymers characterized by the cone and plate rheometer.

Polymers	Molecular Weights			M_w/M_n
	M_w	M_n	M_z	
PP	1.39×10^5 ($\pm 0.08 \times 10^5$)	1.05×10^4 ($\pm 0.20 \times 10^4$)	4.39×10^5 ($\pm 1.41 \times 10^5$)	13.42 ($\pm$ 2.04)
HDPE (1)	1.32×10^5 ($\pm 0.20 \times 10^5$)	1.51×10^4 ($\pm 0.72 \times 10^4$)	8.75×10^5 ($\pm 0.71 \times 10^5$)	10.22 ($\pm$ 6.20)
HDPE (2)	5.29×10^4 ($\pm 0.03 \times 10^4$)	1.66×10^3 ($\pm 0.96 \times 10^3$)	2.41×10^5 ($\pm 0.49 \times 10^5$)	4.12 ($\pm$ 2.64)
PS	1.25×10^5 ($\pm 0.10 \times 10^5$)	5.59×10^4 ($\pm 0.12 \times 10^4$)	1.63×10^6 ($\pm 0.42 \times 10^6$)	2.23 ($\pm$ 0.21)
PMMA	7.94×10^4 ($\pm 0.80 \times 10^4$)	1.13×10^4 ($\pm 0.16 \times 10^4$)	3.31×10^5 ($\pm 0.28 \times 10^5$)	7.04 ($\pm$ 0.18)

3.1.2 Shear Viscosity (η)

The melt viscosities of homopolymers, PP, PS, HDPE(1), HDPE(2), and PMMA as a function of shear strain rate at 200 °C are shown in Figures 3.1(a), 3.1(b), and 3.1(c). At low shear strain rates, the shear viscosities show the Newtonian plateaus, the regions that the shear viscosity is independent of the shear strain rate. For HDPE(1), Newtonian plateau cannot be observed significantly, as shown in Figure 3.1(c). The zero shear rate viscosities, η_o, were obtained by extrapolating the Newtonian plateaus to the zero shear strain rate and are shown in Table 3.2. HDPE(1) has the highest value of the zero shear rate viscosity. HDPE(2) has the lowest value of the zero shear rate viscosity.

Table 3.2 The zero shear viscosity of homopolymers at 200 °C.

Polymers	Zero shear viscosity (P)
PP	$2.09\pm0.05 \times 10^4$
HDPE (1)	$2.30\pm0.40 \times 10^5$
HDPE (2)	$8.43\pm0.50 \times 10^3$
PS	$7.09\pm1.58 \times 10^4$
PMMA	$1.09\pm0.41 \times 10^4$

The shear viscosities of all homopolymers decrease with increasing shear strain rate, indicating that the shear thinning behaviors occur. The shear viscosity of PS is higher than that of PP and HDPE(2) at any strain rates. In the shear strain rate range between 0.1-30 s^{-1}, the shear viscosity of PMMA is lower than that of HDPE(1). Above the shear strain rate of 30 s^{-1}, the shear viscosities of PMMA and HDPE(1) are nearly the same.

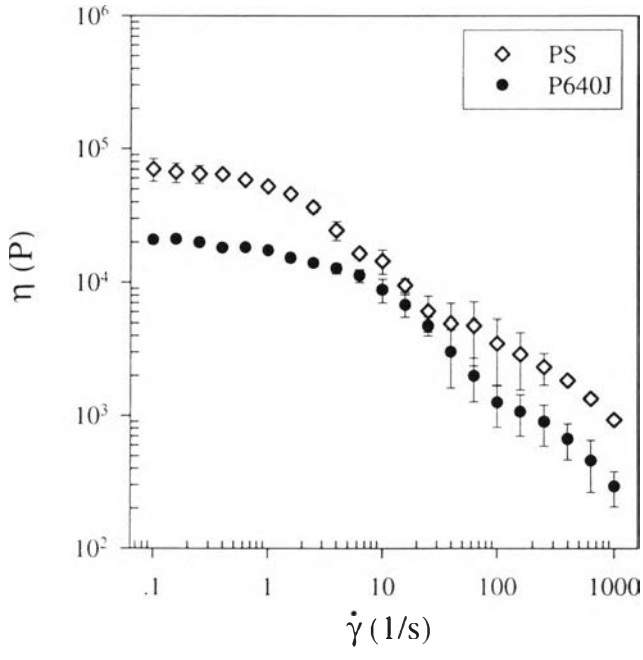

Figure 3.1 (a) The shear viscosities of PP (P640J) and PS as a function of shear strain rate at 200 °C.

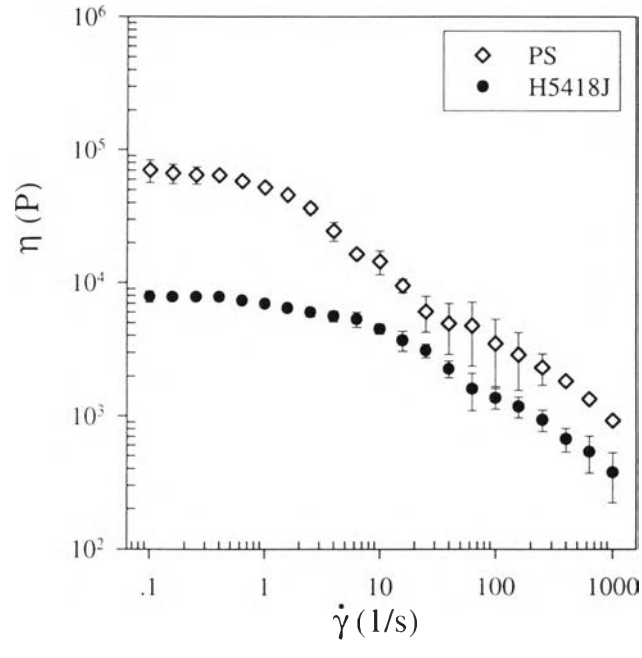

Figure 3.1 (b) The shear viscosities of HDPE (H5418J) and PS as a function of shear strain rate at 200 °C.

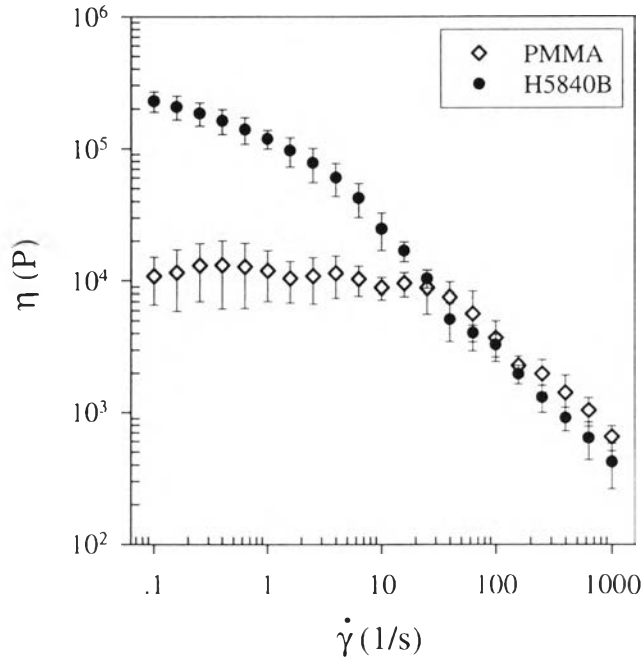

Figure 3.1 (c) The shear viscosities of HDPE (H5840B) and PMMA as a function of shear strain rate at 200 °C.

3.1.3 The First Normal Stress Difference (N_1)

Figures 3.2 (a), 3.2 (b), and 3.2 (c) show the first normal stress differences of homopolymers PP, PS, HDPE(1), HDPE(2), and PMMA as a function of shear strain rate at 200 °C. All the first normal stress differences increase with increasing shear strain rate. The first normal stress difference of PS is higher than those of PP and HDPE(2) at any shear strain rates. While at low shear strain rate, the first normal stress difference of HDPE(1) is higher than that of PMMA. But at the shear strain rates between 40 to 1000 s^{-1}, the first normal stress difference of HDPE(1) is lower than that of PMMA.

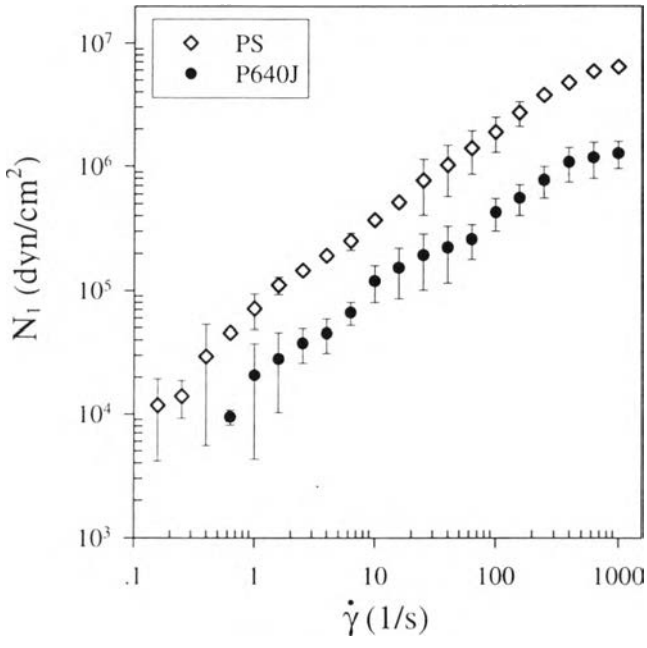

Figure 3.2 (a) The first normal stress differences of PP (P640J) and PS as a function of shear strain rate at 200 °C.

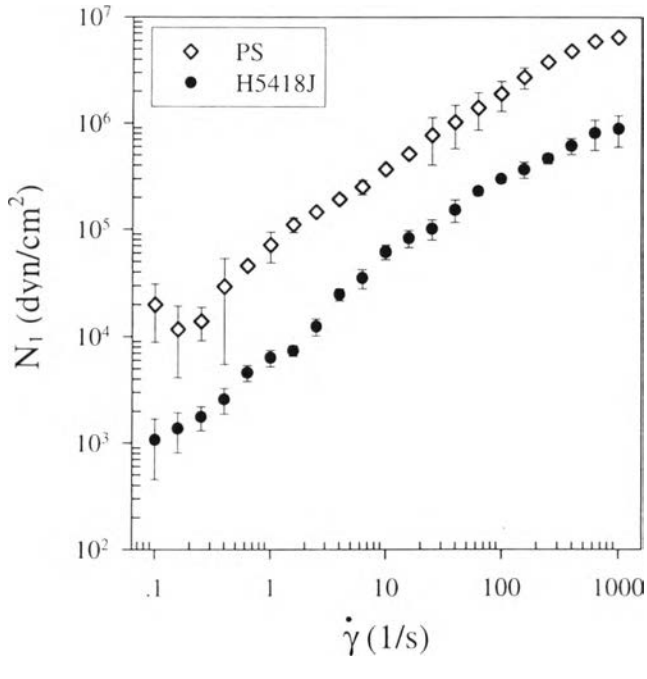

Figure 3.2 (b) The first normal stress differences of HDPE (H5418J) and PS as a function of shear strain rate at 200 °C.

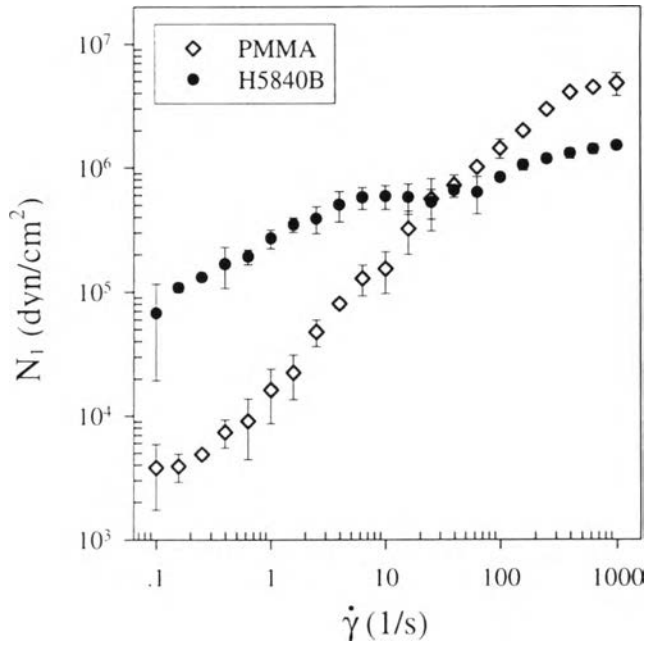

Figure 3.2 (c) The first normal stress differences of HDPE (H5840B) and PMMA as a function of shear strain rate at 200 °C.

The first normal stress difference of polymer melt may have a power-law behavior over a range of shear strain rates (Barnes *et al.*, 1989). If N_1 follows power law, $N_1 = A\ (\dot{\gamma})^m$; where A and m are constant; the constant m varies between 1 to 2 (Barnes *et al.*, 1989). N_1 of PP, PS, HDPE(2), and PMMA measured have the power-law behavior. But N_1 of HDPE(1) does not obey power law over the entire range of strain rate. N_1 has a power law behavior at strain rates, followed by a plateau and non power-law behavior at high strain rates. N_1 as a function of shear strain rate was measured and repeated over 3-7 times. and average values were taken and reported. These data are reproducibility. Several researchers found that N_1 do not always follow the power law behavior (Walters, 1983, and Alvaveg *et al.*, 1985).

3.1.4 The Viscosity Ratio and Normal Stress Ratio of the Blends.

The viscosity ratio (η_r) of the polymer blend is a ratio of the dispersed phase viscosity (η_d) over the matrix phase viscosity (η_m). The shear viscosity data of each phase was characterized individually as a function of shear strain rate, as shown in Figure 3.1. Since the shear viscosity of each homopolymer varies with shear strain rate, so the ratio of shear viscosity is also a function of shear strain rate. The viscosity ratios of the PS/PP blends, the PS/HDPE(2) blends, and the PMMA/HDPE(1) blends as a function of shear strain rate are shown in Figure 3.3. These blend systems provide the viscosity ratios of about 2.0 within shear strain rates between 100 to 1000 s^{-1}. At very low shear strain rate, the viscosity ratios are quite different.

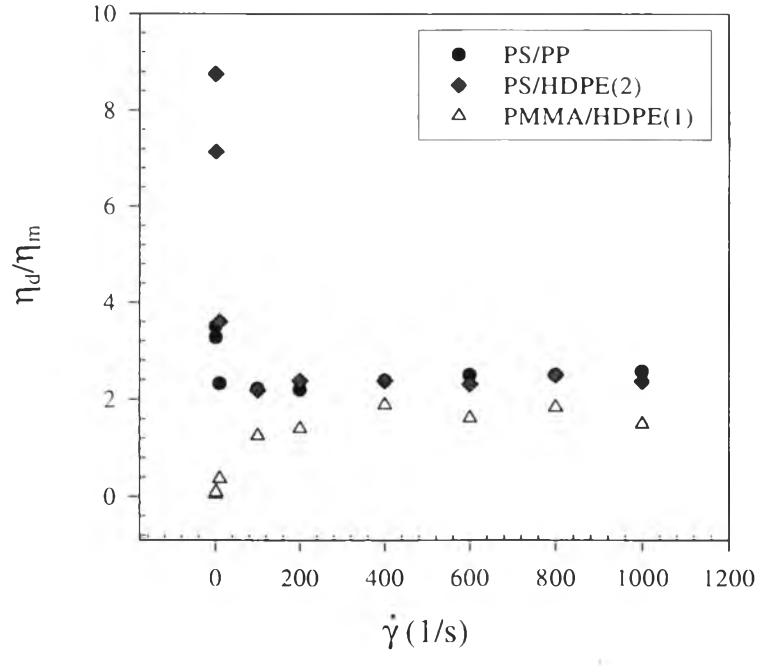

Figure 3.3 The viscosity ratio of the blends as a function of shear strain rate at 200 °C.

The normal stress ratios of the PS/PP blends, the PS/HDPE(2) blends, and the PMMA/HDPE(1) blends as a function of shear strain rate are shown Figure 3.4. They were obtained from the first normal stress differences, which were characterized individually as a function of shear strain rate.

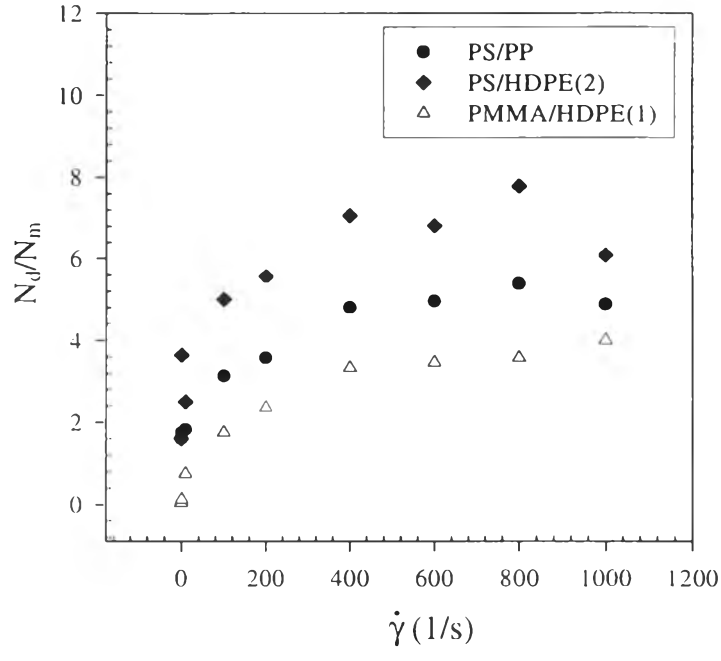

Figure 3.4 The normal stress ratio of the blends as a function of shear strain rate at 200 °C.

The normal stress ratio data of the three blend systems are quite different over the range of shear strain rates. They vary between 2 to 7 amongst the blends. The PS/HDPE(2) blend provides the highest value of the normal stress ratio, whereas the PMMA/HDPE(1) blend shows the lowest value. Because of differences in the viscosity ratio and the normal stress ratio, we can expect different morphologies.

3.1.5 The Complex Moduli G*(ω) of PP and PS

The complex moduli of PP and PS after pre-shearing at shear rates of 1, 10, and 100 s^{-1}, at 200 °C, are shown in Figures 3.5 and 3.6, respectively. The complex moduli of the homopolymer PP at different shearing rates are nearly the same. For the homopolymer PS, the complex moduli at high frequency after shearing at different shear strain rates are equal. But they differ at low frequencies. The reason may come from the changes in

the chain configuration induced by pre-shearing. The complex modulus of PS is lower when it is sheared at a lower shear strain rate.

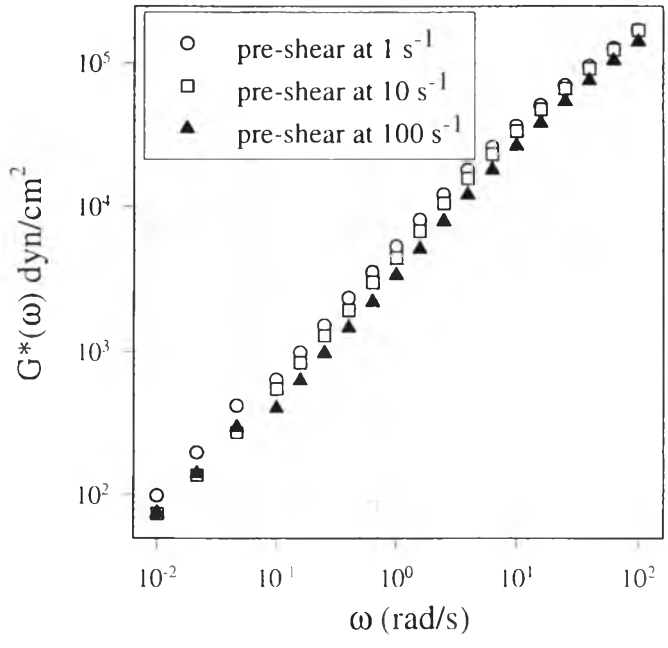

Figure 3.5 The complex modulus G*(ω) of polypropylene as a function of frequency after pre-shearings at 1, 10, and 100 s^{-1}, at 200 °C.

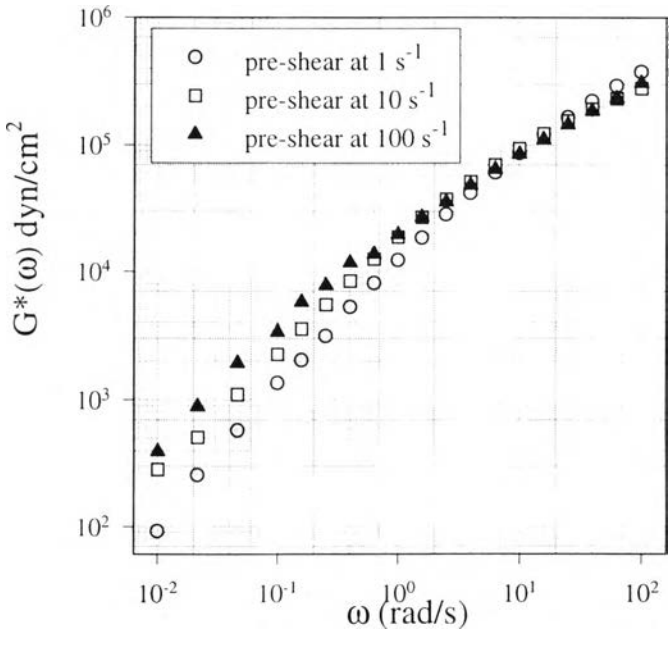

Figure 3.6 The complex modulus G*(ω) of polystyrene as a function of frequency after pre-shearings at 1, 10, and 100 s^{-1}, at 200 °C.

Pre-shearing at the shear strain rate of 1 s^{-1}, the complex modulus is the lowest. Shifting of $G^*(\omega)$ to the higher frequency for pre-shearing at 1 s^{-1} might be due to disentanglement (Dealy, 1990). Homopolymer PS, which has a big bulky group phenylene, is quite stiff. When we applied flow field to the PS melt, the molecular chains moved and disentangled. Additionally, $G^*(\omega)$ of homopolymer PS is higher than that of PP at all frequencies.

3.2 Effect of Shearing Time on Morphology of the PS/PP Blends

The morphology of immiscible blend changes with time during mixing in a twin screw extruder or a batch mixer (Wensheng and Jiasong, 1996). The re-shearing of the blends after mixing would further change morphology as a function of shearing time (Jamieson, 1998). Eventually, they would attain the equilibrium morphology or the equilibrium minor droplet size after a sufficient shearing time.

3.2.1 The Droplet Size versus Dimensionless of Time

The plot of number average diameter of minor phase PS versus the product of shearing time multiplied by shear strain rate at the shear rates of 1, 10, and 100 s^{-1}, at 200 °C are shown in Figure 3.7. At a low shear strain rate, a longer shearing time is required to get the equilibrium morphology. At the shear strain rate of 1 s^{-1}, droplet size of minor phase PS attained equilibrium value after shearing time of 1000 s. At the shear strain rate of 100 s^{-1}, the equilibrium value was obtained within 3 s.

To understand more clearly, the number averaged diameter of minor droplet size over the equilibrium diameter of the PS/PP blends were plotted versus the product of shearing time multiplied by shear rate at the shear rates of 1, 10, 100, and 800 s^{-1}, and are shown in Figure 3.8. This plot shows that the equilibrium droplet size of minor phase is obtained where the

product of shear strain rate multiplied by shearing time exceeds 1000 at any shear rates.

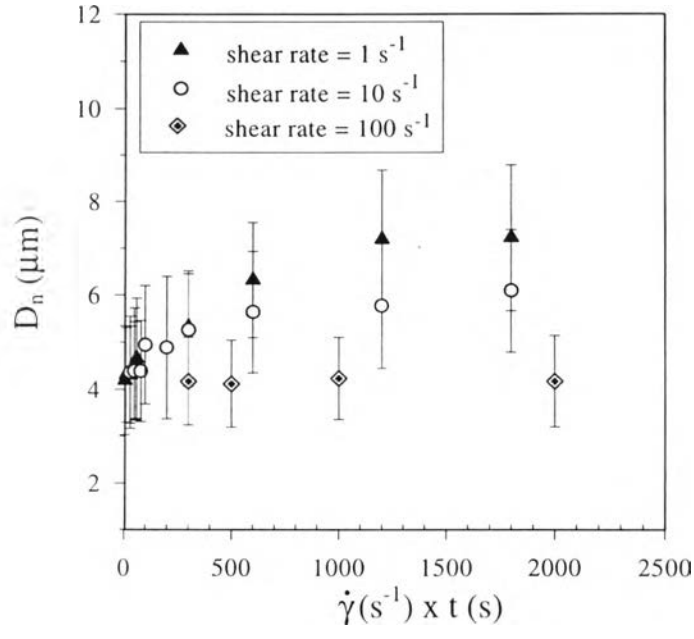

Figure 3.7 The number averaged diameter of minor phase PS versus product of shear strain rate multiplied by shearing time at shear strain rates of 1, 10, and 100 s^{-1}, at 200 °C.

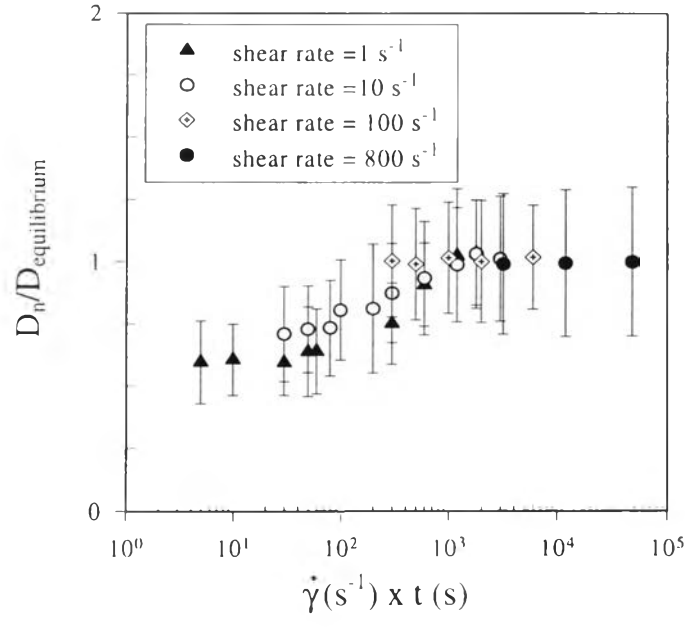

Figure 3.8 The plot of ($D_n/D_{equilibrium}$) versus ($\dot{\gamma}$ x t) of the PS/PP blends at the shear strain rates of 1, 10, 100, and 800 s^{-1}, at 200 °C.

3.2.2 Distribution Function of Droplet Size as a Function of Shearing Time

To investigate the morphology change with shearing time at any shear strain rates, the average droplet sizes do not provide sufficient details or mechanisms involved. So the size distribution functions were determined. The distributions of droplet size as a function of shearing time at the shear strain rates of 1, 10, 100, and 800 s^{-1}, at 200 °C are shown in Figures 3.9 to 3.12, respectively, and can be compared with initial morphology obtained from the brabender mixer.

At the shear strain rates of 1 and 10 s^{-1}, the droplet sizes of minor phase change dramatically with time. At longer shearing time, a bimodal distribution occurs; after a sufficient long shearing time the droplet sizes shift to larger values and attain equilibrium values with a monomodal distribution (shown in Appendix B). At the high shear strain rates of 100 and 800 s^{-1}, the distributions of droplet sizes slightly change with time. At the shear strain rate of 100 s^{-1}, the shifting of droplet sizes does not occur. They show nearly the same sizes as the initial sizes. At the shear strain rate of 800 s^{-1}, the droplet sizes slightly shift to larger values, but no bimodal distribution occurs.

Tables 3.3 (a-d) show the statistical data of droplet size at the shear strain rates of 1, 10, 100, and 800 s^{-1}. These tables consist of the ensemble values, standard deviations, the maximum droplet sizes, and the minimum droplet sizes. We can observe that the broad distributions occur at the long shearing time. The micrographs obtained from optical microscope for the effect of shearing time are shown in Appendix A.

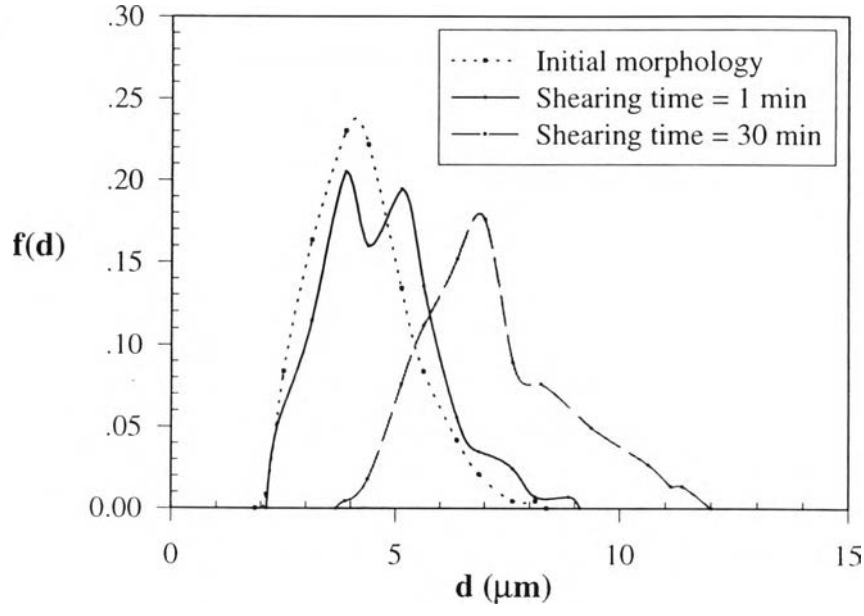

Figure 3.9 Distribution function of droplet size for the PS/PP blends as a function of shearing time at shear strain rate of 1 s^{-1}.

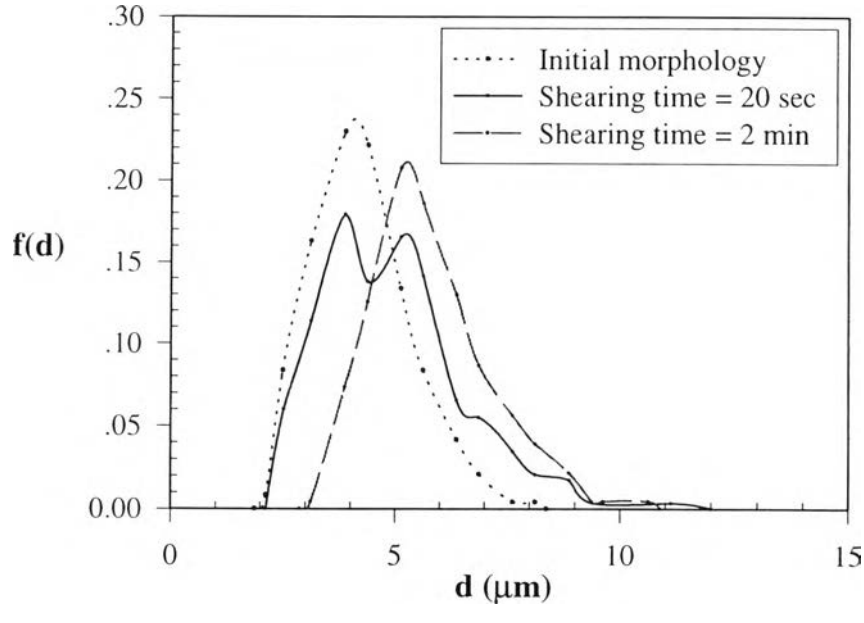

Figure 3.10 Distribution function of droplet size for the PS/PP blends as a function of shearing time at shear strain rate of 10 s^{-1}.

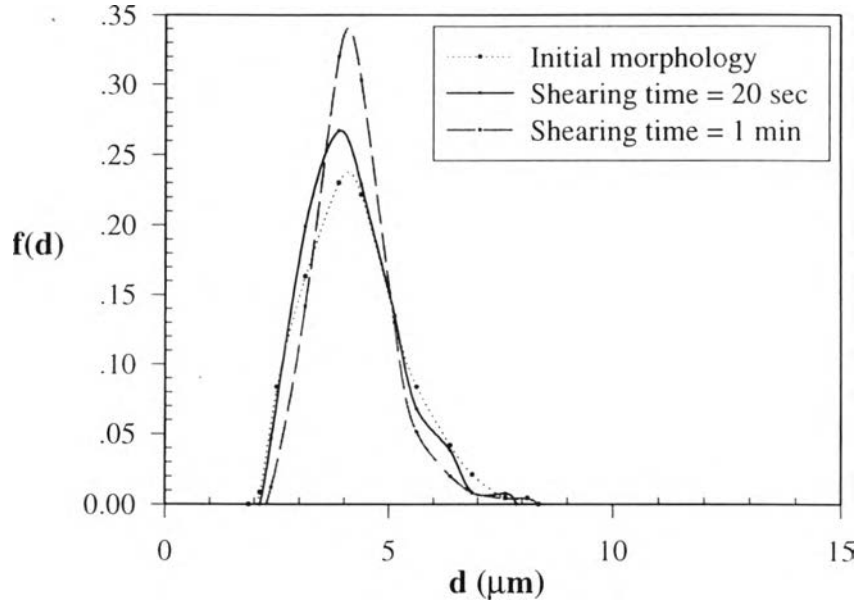

Figure 3.11 Distribution function of droplet size for the PS/PP blends as a function of shearing time at shear strain rate of 100 s^{-1}.

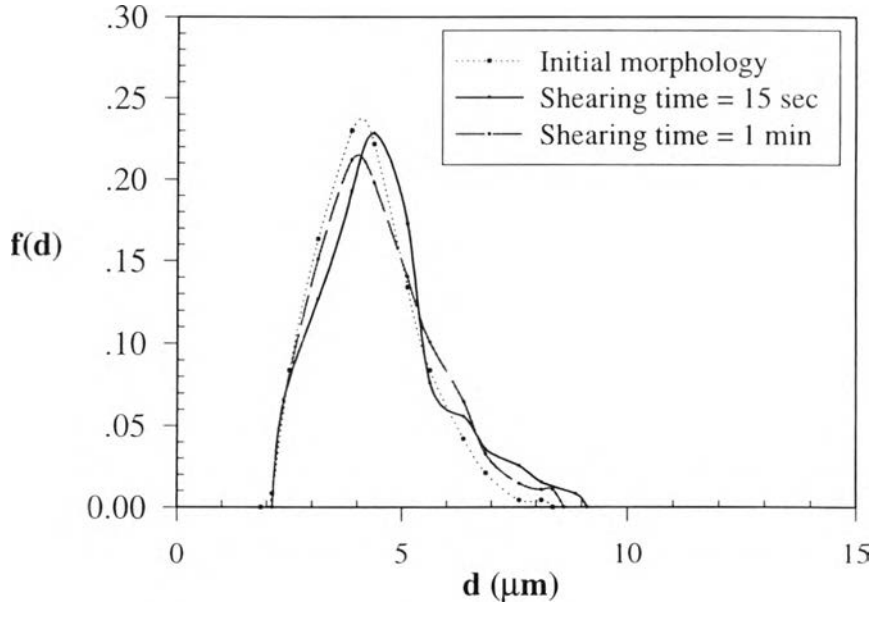

Figure 3.12 Distribution function of droplet size for the PS/PP blends as a function of shearing time at shear strain rate of 800 s^{-1}.

Table 3.3 (a) The ensemble averages of droplet size of the PS/PP blends at the shear strain rate of 1 s^{-1}.

Ensemble averages	Initial drop size	Shearing time							
		5 s	10 s	30 s	50 s	1 min	10 min	20 min	30 min
average (μm)	3.88	4.22	4.31	4.30	4.54	4.66	6.26	7.19	7.22
STD	0.87	1.12	1.00	1.03	1.18	1.27	1.23	1.48	1.58
max (μm)	6.93	8.19	8.19	8.19	8.86	8.86	10.14	11.38	12.71
min (μm)	2.49	2.01	2.01	2.49	2.01	2.49	3.05	3.80	3.80

Table 3.3 (b) The ensemble averages of droplet size of the PS/PP blends at the shear strain rate of 10 s^{-1}.

Ensemble averages	Initial drop size	Shearing time							
		5 s	8 s	10 s	20 s	30 s	1 min	2 min	3 min
average (μm)	3.88	4.38	4.37	4.94	4.86	5.26	5.65	5.77	6.15
STD	0.87	1.05	1.06	1.25	1.50	1.20	1.30	1.32	1.29
max (μm)	6.93	7.57	7.57	8.19	9.42	10.14	10.14	10.71	10.73
min (μm)	2.49	2.49	2.49	2.49	2.49	2.49	3.05	3.05	3.05

Table 3.3 (c) The ensemble averages of droplet size of the PS/PP blends at the shear strain rate of 100 s^{-1}.

Ensemble averages	Initial drop size	Shearing time				
		3 s	5 s	10 s	20 s	1 min
average (μm)	3.88	4.17	4.12	4.24	4.18	4.23
STD	0.87	0.93	0.92	0.88	1.01	0.86
max (μm)	6.93	8.19	7.57	7.57	7.57	8.19
min (μm)	2.49	2.49	2.49	2.49	2.49	2.49

Table 3.3 (d) The ensemble averages of droplet size of the PS/PP blends at the shear strain rate of 800 s^{-1}.

Ensemble averages	Initial drop size	Shearing time		
		4 s	15 s	1 min
average (μm)	3.88	4.41	4.56	4.51
STD	0.87	1.28	1.31	1.32
max (μm)	6.93	8.19	8.86	8.86
min (μm)	2.49	2.49	2.49	2.49

3.3 Effect of Shear Strain Rate on Equilibrium Morphology of the Blends

3.3.1 Equilibrium Droplet Size as a Function of Shear Strain Rate

The effect of shear strain rate on equilibrium droplet size of minor phase was investigated at the shear strain rates of 1 to 800 s^{-1}, at 200 °C, as shown in Figure 3.13. The PS/HDPE(2) blends provide the largest drop sizes of the minor phase at any shear strain rates. The PMMA/HDPE(1) blends provide the smallest drop sizes. The minimum drop sizes of three blend-systems were obtained at the shear strain rate of 200 s^{-1}. Below and above this shear strain rate, the larger drop sizes occurred.

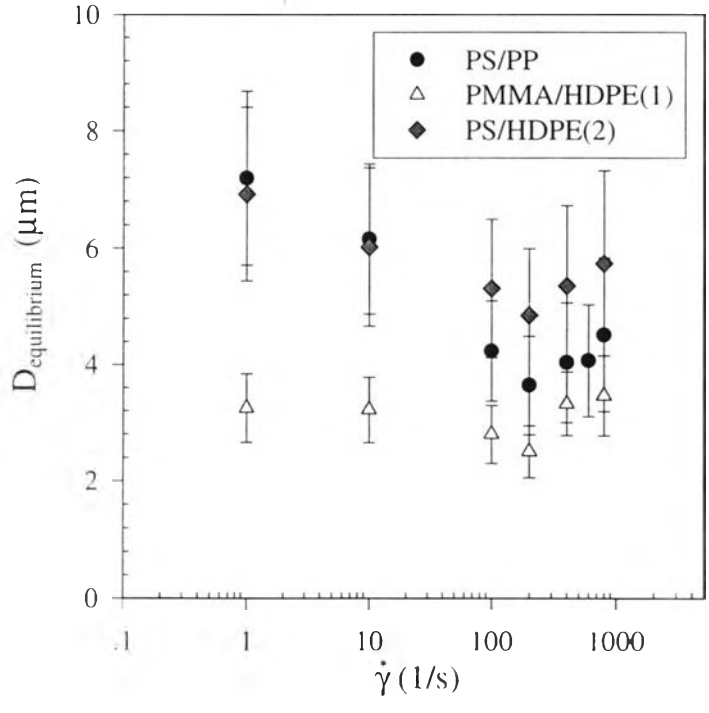

Figure 3.13 The equilibrium droplet size as a function of shear strain rate of the PS/PP blends, the PS/HDPE(2) blends, and the PMMA/HDPE(1) blends at 200 °C.

The interfacial tension has no significant effect on morphology. Generally, a high interfacial tension system is expected to provide the large droplet size of minor phase. For the PMMA/HDPE(1) blends with the highest

value of interfacial tension. they have the smallest droplet sizes at any shear strain rates. Because the viscosity ratio and normal stress ratio of these blends are the lowest, the breakup process was carried out more easily in the blending by the brabender mixer and the shearing by the cone and plate rheometer.

Tables 3.4 (a-c) show the summarized data of the effect of shear strain rates on the equilibrium droplet size compared with the initial sizes from the brabender mixer. All blend systems show that the droplet sizes at the shear strain rates about 100 to 200 s^{-1} are nearly the same as the initial sizes. When the blends were sheared again with the same shear strain rate, the morphology did not change. At high shear strain rate and high shear stress, the droplets were expected to breakup into smaller size, but this was not observed in these studies. As the droplets were broken up, the droplet collisions also occurred due to shear flow. Consequently, the final size of droplets depended on the balancing between the drop breakup and coalescence rates. Our results indicate that the larger droplet sizes occur at high shear strain rates. This means that the rate of coalescence overcame the rate of breakup.

Moreover, coalescence was also encouraged due to mobility of interface between the two phases (at high shear strain rate, high mobility of interface). When coalescence was encouraged, the standard deviations of the droplet sizes were significantly higher.

3.3.2 Distribution Function of Droplet Size as a Function of Shear Strain Rate on Equilibrium Morphology of the Blends.

To observe the progress of the droplets as a function of shear strain rate, the plot of distribution functions are illustrated in Figures 3.14, 3.15, and 3.16. At the shear strain rate of 1 s^{-1}, the droplet size distribution shifts to larger size with broader distribution relative to the initial distribution obtained from the brabender mixer.

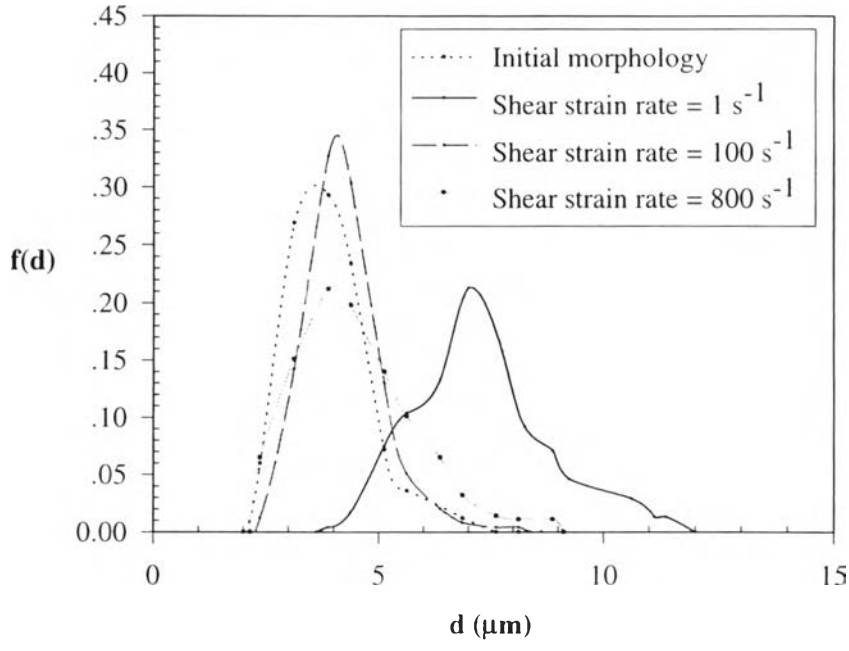

Figure 3.14 Distribution function of droplet size of the PS/PP blends as a function of shear strain rate at 200 °C.

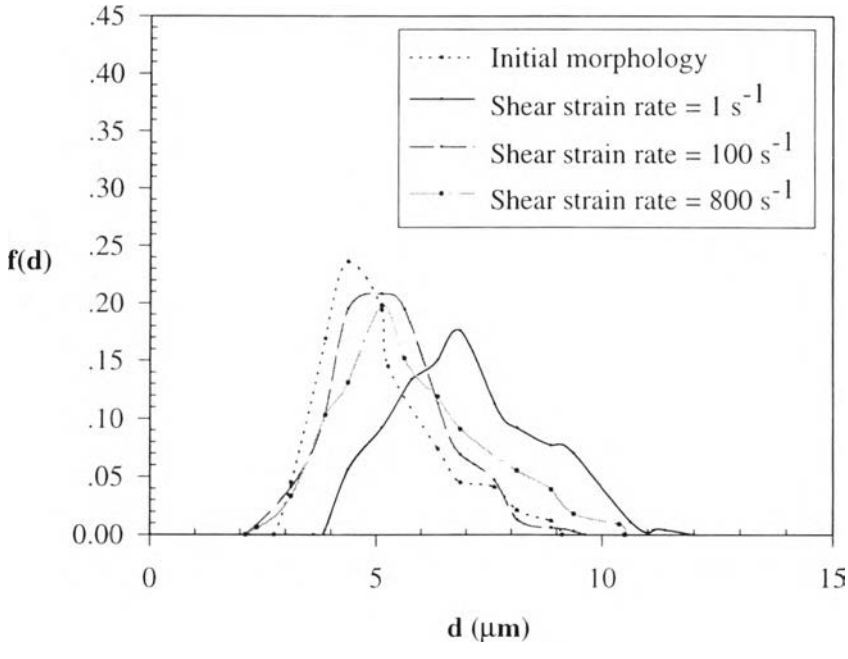

Figure 3.15 Distribution function of droplet size of the PS/HDPE(2) blends as a function of shear strain rate at 200 °C.

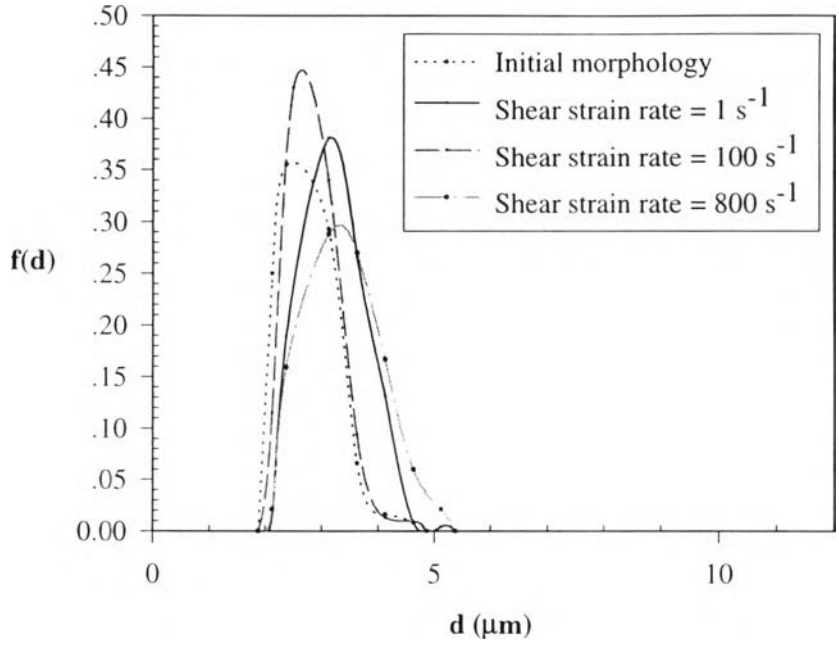

Figure 3.16 Distribution function of droplet size of the PMMA/HDPE(1) blends as a function of shear strain rate at 200 °C.

At the shear strain rate of 800 s^{-1}, the distribution of drop is broad with nearly the same minimum drop sizes as the initial drop sizes. The following Figure 3.17 shows the explanation above.

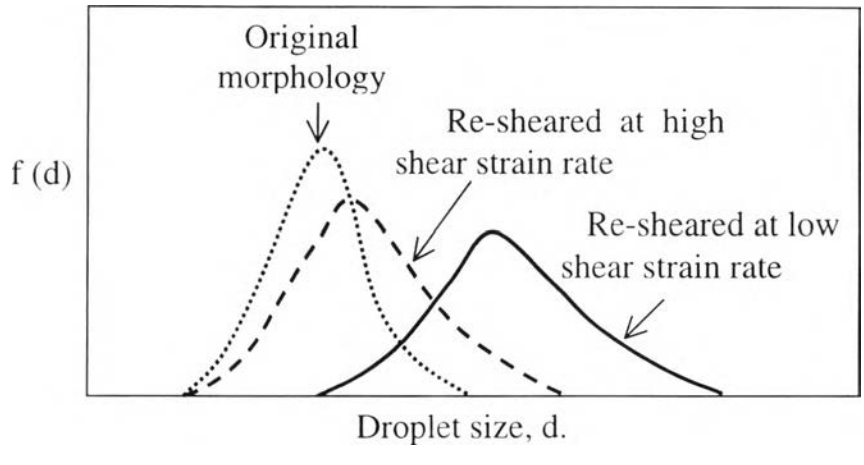

Figure 3.17 Droplet size distribution as a function of shear strain rate.

Micrographs of three blend systems in the effect of shear strain rate on equilibrium morphology are shown in Appendix A.

Table 3.4 (a) The ensemble averages of equilibrium droplet size of the PS/PP blends as a function of shear strain rate.

Ensemble averages	Initial droplet size	Shear strain rate (1/s)					
		1	10	100	200	400	800
average (μm)	3.88	7.19	6.15	4.23	3.66	4.03	8.51
STD	0.87	1.48	1.29	0.86	0.85	1.03	1.32
max (μm)	6.93	11.38	10.73	8.19	6.93	6.93	8.86
min (μm)	2.49	3.80	3.05	2.49	2.49	2.49	2.49

Table 3.4 (b) The ensemble averages of equilibrium droplet size of the PS/HDPE(2) blends as a function of shear strain rate.

Ensemble averages	Initial droplet size	Shear strain rate (1/s)					
		1	10	100	200	400	800
average (μm)	5.08	6.92	6.02	5.31	4.84	5.35	5.03
STD	1.23	1.49	1.35	1.19	1.15	1.37	1.58
max (μm)	8.86	11.38	11.38	9.42	8.47	10.14	10.73
min (μm)	3.05	3.80	3.80	3.05	2.49	2.49	2.49

Table 3.4 (c) The ensemble averages of equilibrium droplet size of the PMMA/HDPE(1) blends as a function of strain rate.

Ensemble averages	Initial droplet size	Shear strain rate (1/s)					
		1	10	100	200	400	800
average (μm)	2.66	3.25	3.21	2.79	2.46	3.34	3.41
STD	0.54	0.55	0.59	0.49	0.43	0.54	0.67
max (μm)	4.64	5.10	5.64	4.64	4.09	4.64	5.10
min (μm)	2.03	2.03	2.03	2.03	2.03	2.03	2.03

3.4 Effect of Initial Conditions on Equilibrium Morphology of the Blends

The effect of initial conditions on equilibrium morphology as a function of shear strain rate was investigated. Figure 3.18 shows the equilibrium droplet size of minor phase PS of the PS/PP blends as functions of shear rate and the brabender mixing speed at 200 °C.

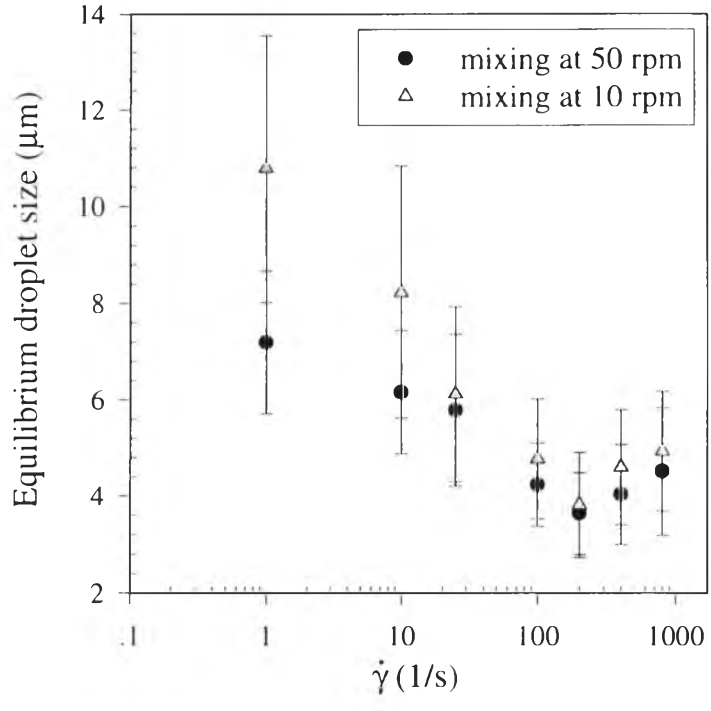

Figure 3.18 The equilibrium droplet size of minor phase PS of the PS/PP blends as functions of shear strain rate and mixing speed at 200 °C.

Different mixing conditions were obtained by varying the speed of the mixer at the fixed temperature of 200 °C. The results indicate that the equilibrium droplet sizes at the shear strain rates of 1 and 10 s^{-1} from mixing with speeds of 10 and 50 rpm are different. The equilibrium droplet sizes for the shear strain rates between 25 to 800 s^{-1} for both mixing speeds are nearly the same but for the mixing speed of 10 rpm the droplet sizes are slightly larger. The standard deviations of the droplet sizes for both mixing speeds are

higher when the blends were subsequently sheared at lower shear strain rates. It can be concluded that at low shear rates the equilibrium morphology remembers the history of the blending that so called "*hysteresis*". Because we want to relate between the morphology parameters and viscoelastic properties, the hysteresis data will now be excluded from the correlation.

3.5 The Correlation between Viscoelasic Properties and Morphology of the Immiscible Blends

The morphology of immiscible blend depends on mixing conditions, rheological properties, and thermodynamic properties. The dimensionless capillary number (Ca), was used to indicate the ratio of shear force over interfacial tension force, $(\eta_m \dot{\gamma})/(2\Gamma/D)$. The other dimensionless parameters, such as viscosity ratio (η_d/η_m) and normal stress ratio (N_d/N_m), were used to correlate with Ca.

3.5.1 The Capillary Number (Ca) and Viscosity Ratio (η_r) Correlation

Figure 3.19 shows the correlation between Ca and η_r of the PS/PP blends, the PS/HDPE(2) blends, and the PMMA/HDPE(1) blends at shear strain rates between 25 to 800 s^{-1}, at 200 °C. The hysteresis data were excluded from this correlation. Taylor's predictions and Wu's predictions of Ca as a function of viscosity ratio were also plotted in this figure. It can be seen that the experimental data are quite different from Taylor's predictions. Taylor's theory was derived based on Newtonian system without elastic effect. The capillary numbers Ca of experiment are higher than the Taylor's prediction, because the polymer blends are viscoelastic systems, requiring higher shear force to balance the restoring surface tension. When the experimental data are compared with Wu's prediction, they agree at viscosity ratios between 1 to 2. For viscosity ratio above 2, the experimental data do

not fit Wu's correlation. The experimental Ca values are higher than Wu's predictions. Wu's correlation was obtained from the blend systems sheared only at 100 s^{-1}. It cannot account for the *shear-induced coalescence* and the elastic effect at high shear rates.

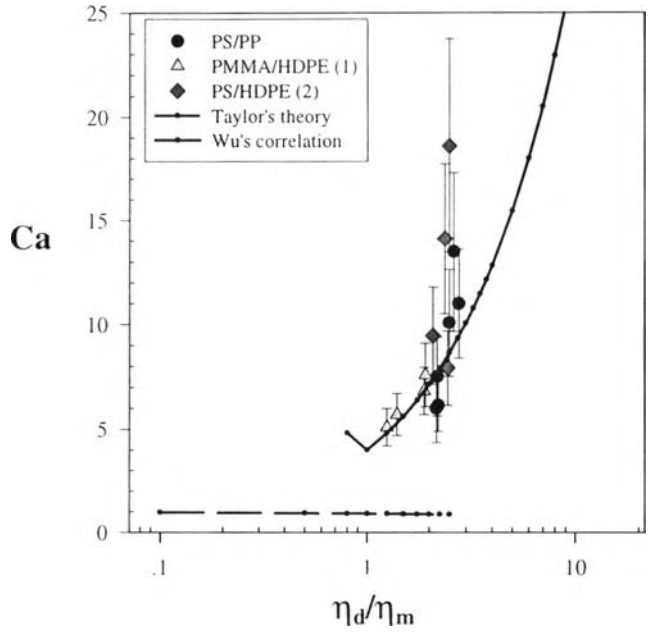

Figure 3.19 The correlation between a capillary number (Ca), and viscosity ratio (η_d/η_m) of the PS/PP blends, the PS/HDPE(2) blends, and the PMMA/HDPE(1) blends at 200 °C.

The minimum Ca of our experiment is about 5. The PMMA/HDPE(1) blends, at the shear rate of 100 s^{-1}, have low values for Ca, because their viscosity ratio is the lowest: about 1.7 (Wu, 1987, and Utracki, 1992). Clearly their correlation is not appropriate for our blends and the conditions used.

3.5.2 The Capillary Number (Ca) and Normal Stress Ratio (N_r) Correlation

Figure 3.20 shows the correlation between the capillary number and the normal stress ratio as determined by equivalent shear strain rates

between the matrix and the minor phases, of the PS/PP blends, the PS/HDPE (2) blends, and the PMMA/HDPE(1) blends at shear strain rates between 25 to 800 s^{-1}. This correlation was tested and it includes both the viscous and elastic properties of the blends. The viscous property is included in term of Capillary number. It gives a better correlation compared with Ca versus η_r. The minimum value of Ca is about 5. At $N_1 > 3$, the capillary number seems to vary with N_1 and the data do not collapse well.

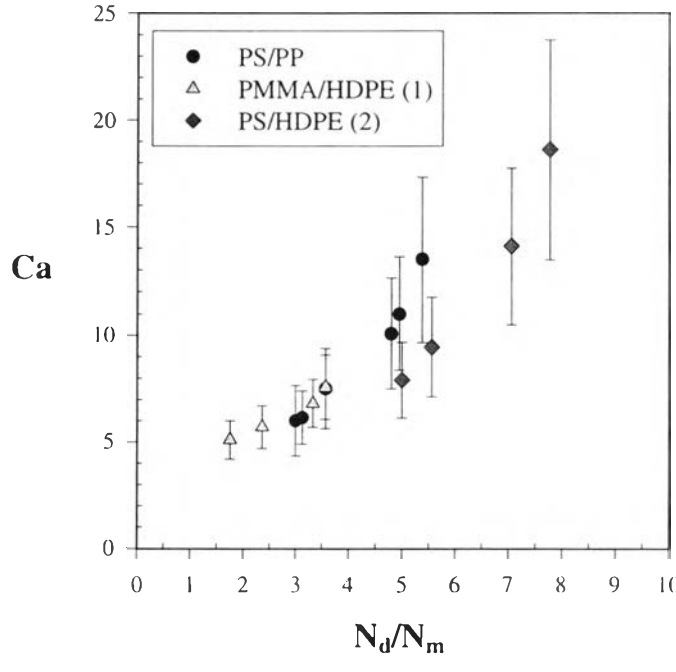

Figure 3.20 The correlation between a capillary number (Ca) and the normal stress ratio (N_d/N_m) by means of shear strain rate of the PS/PP blends, the PS/HDPE(2) blends, the PMMA/HDPE(1) blends at 200 °C.

When two polymers, having different viscoelastic properties (viscosity and the first normal stress difference), are mixed together, the rheological behaviors of two phases must be different when shear stress is applied. Essentially, the shear strain rates of two phases must be different because of a difference in viscosity. But the shear stresses of both phases should be equal, base on the assumptions of no slip at the interface and that the

stress distribution is uniform. The following figure depicts the schematic explanation above. When we apply shear stress to the blend system, the stress will be distributed in the matrix phase first, and simultaneously it is transferred to the minor phase. Both phases will flow in the direction of shear force, but they do not flow at the same shear strain rate because of the difference in viscosity.

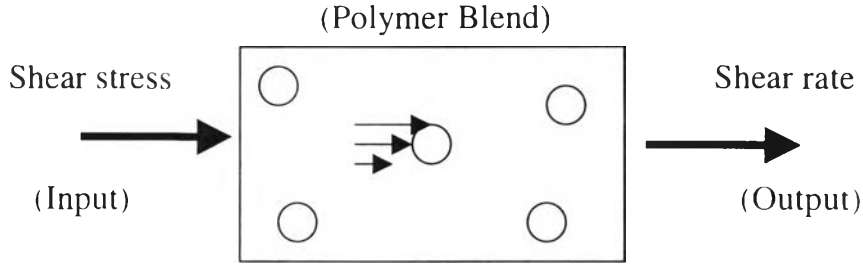

$\dot{\gamma}$of dispersed phase $\neq$ $\dot{\gamma}$of matrix phase: $\eta_d \neq \eta_m$

$$\tau = \tau_m = \tau_d$$

Figure 3.21 The schematic explanation for the meanings of normal stress ratio of the immiscible blends.

To make the correlation of this, a new correlation of Ca versus normal stress ratio as determined by equivalent shear stresses is required. The correlation data with and without correction are tabulated in Appendix D.

3.5.3 The Capillary Number (Ca) and Normal Stress Ratio Correction (N_r') Correlation

Figure 3.22 shows the correlation between Ca and N_r' (N'_d / N_m) of the PS/PP blends, the PS/HDPE(2) blends, and the PMMA/HDPE(1) blends at shear strain rates between 25 to 800 s^{-1}, at 200 °C. This plot excludes the hysteresis data. There is a good relation between Ca and N_r'. At $N_r' > 3$, Ca increases with N_r'. When $N_r' < 3$, Ca seems to settle down to a constant value of about 5. The viscous force required to produce this droplet size is five

times the surface tension if $N_r' < 3$. For $N_r' > 3$, the elasticity of drop is very large, so the breakup process is more difficult to occur even at high shear rates. Although droplets can be broken up due to applied shear force, they can also collide and coalesce during flow: competition between breakup and coalescence processes (Utracki, 1991). Our results show that coalescence is favorable at high shear strain rates. So increasing Ca with the normal stress ratio (N_r') is obtained.

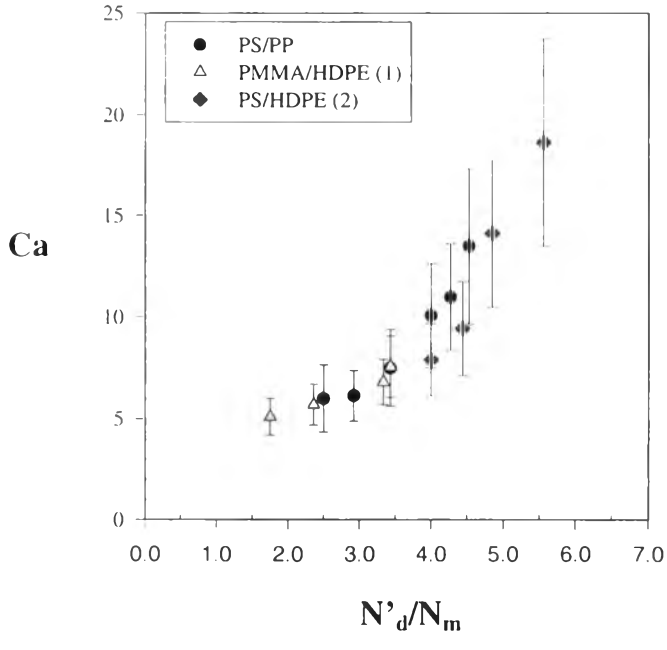

Figure 3.22 The correlation between a capillary number (Ca) and the normal stress ratio (N'_d/N_m) by means of shear stress of the PS/PP blends, the PS/HDPE(2) blends, and the PMMA/HDPE(1) blends at 200 °C.

At low shear strain rates and low normal stress ratios, coalescence also occurs. When the low shear stress was applied to the low elastic drops, it is too low to break them into smaller sizes. As shearing force was applied to the blend systems again, it favored and generated coalescence (Jamieson, 1998).

3.6 Palierne's Theory

Palierne recently described the linear viscoelastic behavior of a viscoelastic material dispersed in an incompatible viscoelastic liquid in the presence of an interfacial agent (Palierne, 1990). When we apply small oscillatory strain to a blend system, it does not affect the overall morphology, the shape of the dispersed phase is only slightly perturbed. This theory takes into account the deformation and relaxation of the shape of dispersed phase for calculation of the viscoelastic properties of the emulsion. Equation 3.1 shows the viscoelastic constitutive equation of Palierne's theory. Hence, dynamic measurements can serve as a technique for determining the complex modulus of blends by fitting this equation to the experimental data, provided the droplet radius of the blend can be determined by an independence method. The interfacial tension must also be known. In the present study, Palierne's theory will be compared with the experimental data to test whether this theory can be used for an incompatible blend without interfacial agent.

This dynamic viscoelastic constitutive equation is functions of the linear viscoelastic behavior of two phases, the size distribution of droplet, and the interfacial tension (Palierne, 1990):

$$G^*(\omega)_{system} = G^*(\omega)\ \frac{1+3\sum_i \phi_i H_i(\omega)}{1-2\sum_i \phi_i H_i(\omega)} \qquad (3.1)$$

where

$$H_i(\omega) = \left\{ \frac{4(\Gamma/R_i)\left[2G_m^*(\omega)+5G_i^*(\omega)\right]+\left[G_i^*(\omega)-G_m^*(\omega)\right]\left[16G_m^*(\omega)+19G_i^*(\omega)\right]}{4(\Gamma/R_i)\left[G_m^*(\omega)+G_i^*(\omega)\right]+\left[2G_i^*(\omega)+3G_m^*(\omega)\right]\left[16G_m^*(\omega)+19G_i^*(\omega)\right]} \right\}$$

$G^*_i(\omega)$, $G^*_m(\omega)$, and $G^*(\omega)$ are, respectively, the complex moduli of dispersed phase, matrix phase, and the emulsion at frequency ω. Γ is the interfacial tension, ϕ_i is the volume fraction of inclusions of radius R_i.

The complex moduli of the PS disperse, the PP matrix, and the PS/PP blends were measured after cessation of steady state shear flow. The moduli then reflect the structures that have been generated during the previous steady state shearing, called "*pre-shearing*". Pre-shearing for a sufficient long time gives the equilibrium morphology, as can be referred to the results of our experiment in section 3.2.

3.6.1 Effect of Shear History on Complex Modulus of the PS/PP Blends.

The complex moduli of PS/PP blends as functions of frequency and pre-shearing are shown in Figure 3.23. Pre-shearing at different shear strain rates can affect and alter the size of dispersed phase. At the shear rate of 1 s^{-1}, the droplet size PS is largest; at pre-shearing of 200 s^{-1}, the smallest droplet size was obtained, as shown in Table 3.4. This figure shows that the complex modulus G*(ω) of the PS/PP blends at 200 °C increases significantly as the dispersed size increases.

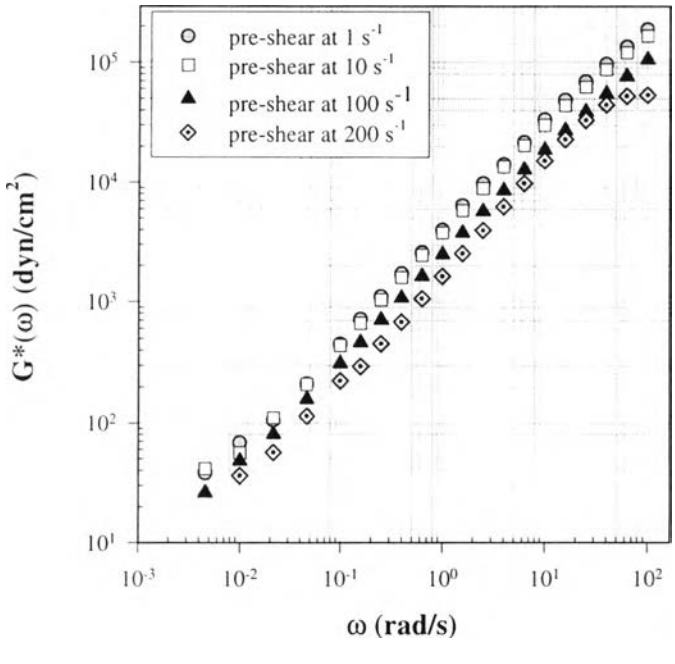

Figure 3.23 The complex modulus G*(ω) as a function of frequency for the PS/PP blends after pre-shearing at 1, 10, 100, and 200 s^{-1}, at 200 °C.

Additionally, $G^*(\omega)$ of the blends depends on relaxation time of minor phase drop (Doi and Ohta, 1991). The relaxation time is proportional to the droplet size. For the large droplet size, the relaxation time is high causing the rising in $G^*(\omega)$. This result is in agreement with previous work of Vinckier (1998).

3.6.2 Comparison of the Experimental Complex Modulus of the PS/PP Blend with the Prediction of Palierne's Theory

The moduli of the PS/PP blends after pre-shearing at different shear strain rates were compared directly with the Palierne model (Eq. 3.1). The experimental complex modulus of the PS/PP blends and predicted values by Palierne's equation were plotted and are shown in Figures 3.24 (a-c). It can be seen that the theory does not fit well in the low frequency range. The complex moduli of experimental data are lower than the theory. In the high frequency range, experimental $G^*(\omega)$ agrees with the theoretical result. It is suggested that the deviation from theory might come from the measuring conditions used. At low frequencies, 0.01-0.5 rad/s, 100% strain was used to attain measurable values of torque. This high % strain may cause the overall blend morphology to change even at low deformation rate. The effect of % strain on complex modulus of the blend is illustrated in the section 3.6.3.

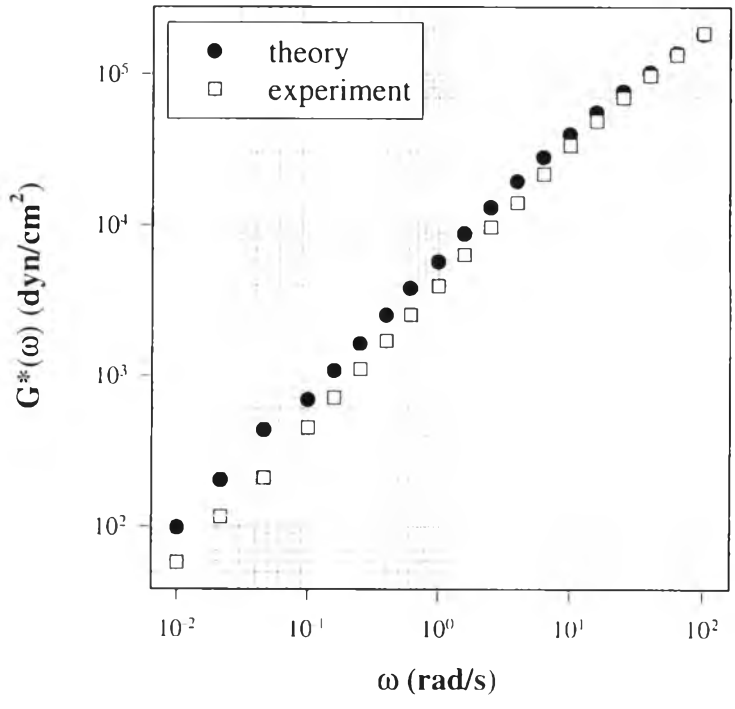
theory
experiment
G*(ω) (dyn/cm²)
ω (rad/s)

(a)

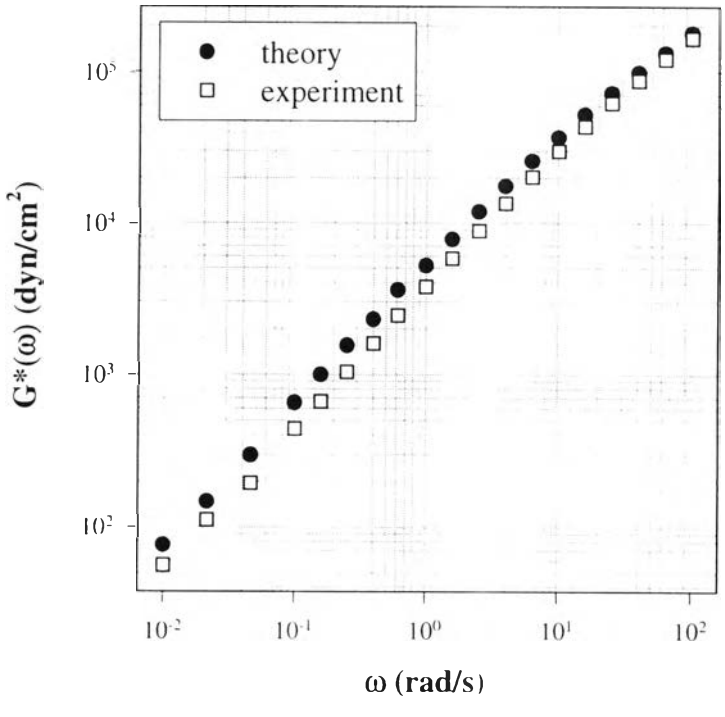
theory
experiment
G*(ω) (dyn/cm²)
ω (rad/s)

(b)

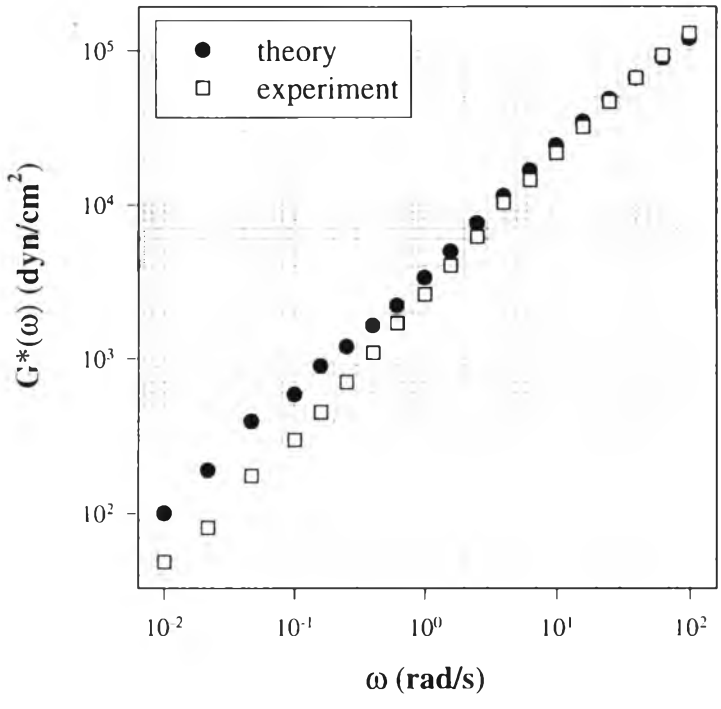

(c)

Figure 3.24 (a-c) The comparison between experimental data and the predicted values by Palierne's theory of complex modulus G*(ω) for the PS/PP blends (a) at pre-shearing of 1 s^{-1}, (b) at pre-shearing of 10 s^{-1}, and (c) at pre-shearing of 100 s^{-1}, at 200 °C.

3.6.3 Effect of % Strain on Complex Modulus of the PS/PP Blends

The effect of %strain on linear viscoelastic properties was investigated through the complex modulus at strains of 10%-100% which were used to measure G*(ω) as a function of frequency at 200 °C. Figure 3.25 shows the plot between G*(ω) of the PS/PP blends after pre-shearing at 100 s^{-1} at 200 °C. Reduction in G*(ω) at 100% strain occurs at all frequencies. The complex moduli for the conditions of 10%, 20%, and 50% strains are nearly the same. The level of the decrease in G*(ω) at 100% strain depends on frequency. At high frequency, the reduction of G*(ω) is relatively higher than at low frequency. At high oscillatory amplitude and oscillatory rate, G*(ω) of

the PS/PP blends is relatively more reduced as a result of deformation in small scale structures away from equilibrium (Graebling *et al.*, 1993).

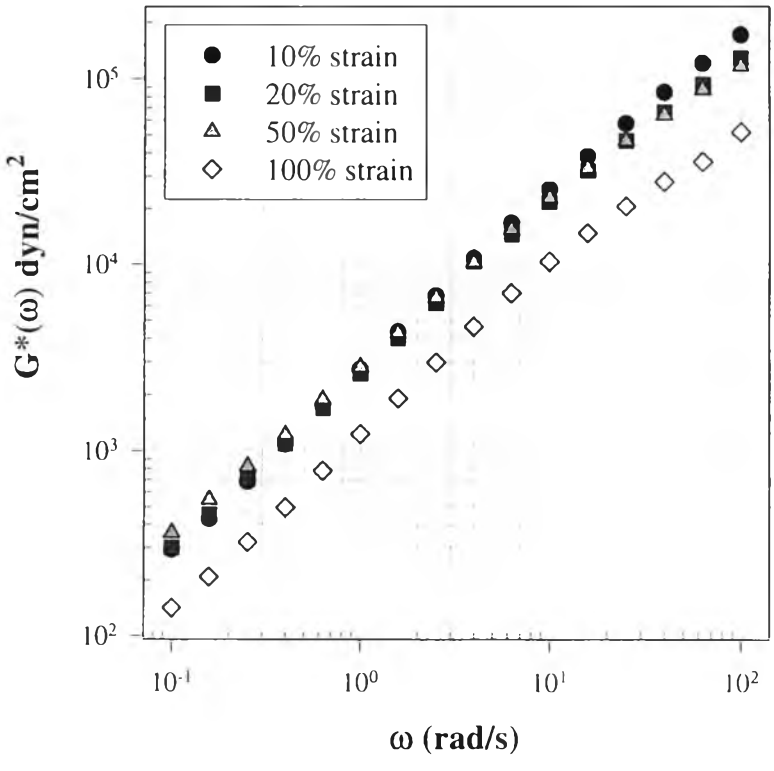

Figure 3.25 The effect of % strain on complex modulus G*(ω) of the PS/PP blends after pre-shearing at 100 s^{-1} at 200 °C.